Brown carbon is a significant contributor to aerosol climate forcing in the northwestern Himalayas

Rahul Kant Yadav[a,#], Aditi Rana[a,#], Rajdeep Singh[b], Harish C. Phuleria[b], Sayantan Sarkar[a]*

[a]School of Civil and Environmental Engineering, Indian Institute of Technology (IIT) Mandi, Kamand, Himachal Pradesh 175005, India.

[b]Environmental Science and Engineering Department, and Centre for Climate Studies, Indian Institute of Technology Bombay (IIT), Mumbai, Maharashtra 400076, India

[#]these authors contributed equally

*Corresponding author at: Room No. A11-05-38, Indian Institute of Technology (IIT) Mandi, Kamand, Himachal Pradesh 175005, India; Email: sayantan@iitmandi.ac.in

Supplementary information

Contains 23 pages, 7 tables and 9 figures

1. Methodological details

1.1 Aerosol neutralization factor (Nf)

The neutralization factor (Eq. S1) identifies the major neutralizing agent in the study area and is calculated as below.

$$Nf = \frac{[cation]}{\left[SO^{2-}_{4}\right] + [NO^{-}_{3}]} \quad \text{(S1)}$$

Neutralisation factor of cations for all seasons is given in Table S5.

1.2 PMF data preparation, choice of factors and error estimation

Outliers beyond three standard deviations for each species were excluded. The signal-to-noise ratios for each input variable exceeded 3, and consequently all variables were

categorized as “strong” in the initial analysis. The sum of all variables was termed the “total variable” and was considered “weak”. The dataset was tested for PMF solutions ranging from 2 to 10 factors, with each run being repeated 20 times. The final number of factors was chosen based on how interpretable each solution was, the variation in Q/Q_{exp} with different factor numbers, and result of robustness assessments. Q/Q_{exp} values consistently decreased without reaching a minimum for 2-10 factor runs. From the analysis of residuals of the initial runs, variables with scaled residuals outside ±3 that adversely affected the results were labelled as "weak." Factor solutions were then re-run and it was observed that the rate of decline in Q/Q_{exp} reduced beyond the 4-factor solution, and factor profiles were split from the 5-factor solution onwards. In the 4-factor solution, the regression coefficient (R^2) for the modelled versus observed total variable was 0.98, suggesting strong model performance. This solution was thus considered optimal for the dataset based on these findings and the physical interpretation of source profiles. The stability of Q for the 4-factor solution was assessed through 20 iterations with random seeds. Rotational ambiguity was examined using the Fpeak function, by testing Fpeak values from -0.5 to +1.5 in 0.5 increments for the 4-factor solution. The Q/Q_{exp} and Q_{robust}/Q_{true} reached clear minima at Fpeak = -0.5 (dQ = 6.6%), leading to the selection of this Fpeak value for rotation application. Two error estimation methods, displacement (DISP) and bootstrapping (BS), were applied to the PMF solution. No factor swaps were detected in DISP for dQmax=4, 8, 15, and 25, suggesting that the stability of the PMF solution was acceptable. A total of 100 BS runs were conducted with a minimum correlation coefficient criterion of 0.6. For both the base factor and Fpeak factor solutions, 90-100% of BS factors corresponded to base/Fpeak factors, demonstrating the solution's robustness (Table S2).

Table S1. Seasonal averages of temperature, relative humidity, wind speed, and wind direction during the study period.

Parameter	Summer	Post-monsoon	Winter
Wind speed (m s^{-1})	4.1 ± 0.6	4.5 ± 1.3	2.3 ± 0.3
Wind direction (degree)	180.1 ± 105.8	150.1 ± 97.4	154.8 ± 88.2
RH (%)	73.6 ± 9.5	75.0 ± 12.0	69.2 ± 13.1
Temperature (°C)	21.2 ± 4.5	19.1 ± 5.1	8.0 ± 1.8

Table S2. Diagnostics of error estimation from BS mapping and DISP for the base run, and BS mapping for the Fpeak run.

BS Mapping: (R ≥ 0.6) (Base run)		Crustal	Secondary	Biomass	Fossil fuel	Unmapped
Crustal		100	0	0	0	0
Secondary		2	78	17	3	0
Biomass		0	0	97	3	0
Fossil fuel		0	1	0	99	0
DISP Diagnostics (Base run)			Error code: 0 Largest Decrease in Q: 0			
Factor Swaps	dQmax = 4	0	0	0		
	dQmax = 8	0	0	0		
	dQmax = 15	0	0	0		
	dQmax = 25	0	0	0		
BS Mapping: (R ≥ 0.6) (Fpeak value: -0.5)		Crustal	Secondary	Biomass	Fossil fuel	Unmapped
Crustal		100	0	0	0	0
Secondary		0	97	3	0	0
Biomass		0	0	99	1	0
Fossil fuel		0	0	0	100	0

Table S3. Sensitivity analysis of Relative Radiative Forcing with changing planetary boundary layer (PBL) height and mass absorption efficiency (MAE) of elemental carbon (EC).

	% Change		
MAE (m^2 g^{-1})	300-400 nm	300-700 nm	300-2500 nm
6	24.8	24.9	24.9
6.5	15.3	15.3	15.3
7	7.1	7.1	7.1
7.5	0.0	0.0	0.0
8	-6.2	-6.2	-6.2
8.5	-11.7	-11.7	-11.7
9	-16.5	-16.6	-16.6
	% Change		
PBL (m)	300-400 nm	300-700 nm	300-2500 nm
700	-0.17	-0.13	-0.11
800	-0.11	-0.09	-0.07
900	-0.06	-0.04	-0.04
1000	0.00	0.00	0.00
1100	0.06	0.04	0.04

1200	0.11	0.09	0.07
1300	0.17	0.13	0.11

Table S4. POC and SOC estimates (µg m^{-3}) using three methods: i) the $(OC/EC)_{min}$ method; ii) the regression-based (15^{th} percentile method); and iii) the MRS method across seasons.

Season	Method	POC (µg m^{-3})	SOC (µg m^{-3})
Summer	$(OC/EC)_{min}$	1.96 ± 0.7	3.19 ± 0.1
	Regression	2.17 ± 0.8	2.9 ± 1.0
	MRS	1.5 ± 0.6	3.6 ± 1.0
Post-Monsoon	$(OC/EC)_{min}$	3.4 ± 1.24	2.9 ± 0.7
	Regression	4.6 ± 1.7	1.5 ± 0.8
	MRS	3.8 ± 1.4	2.4 ± 0.8
Winter	$(OC/EC)_{min}$	4.2 ± 1.7	7.3 ± 3.7
	Regression	8.6 ± 3.7	2.6 ± 2.4
	MRS	9.8 ± 4.3	1.5 ± 1.9

Table S5. Neutralisation factor (Nf) of cations.

Nf	NH_4^+	K^+	Ca^{2+}	Mg^{2+}
Summer	1.00 ± 0.51	0.33 ± 0.17	0.04 ± 0.02	0.09 ± 0.06
Post-monsoon	1.06 ± 0.29	0.49 ± 0.30	0.42 ± 0.20	0.04 ± 0.02

Winter	0.58 ± 0.37	0.29 ± 0.15	0.21 ± 0.15	0.06 ± 0.04

Table S6. Summary of optical parameters of water-soluble and methanol-soluble brown carbon (BrC_{aq} and BrC_{me}) reported for the Himalayan region. Here, b_{abs_365} is the absorption coefficient at 365 nm, MAE_{365} is the mass absorption efficiency at 365 nm, and AAE is the absorption Ångström exponent.

Location	Altitude	Region	Season	BrC_{aq}			BrC_{me}			Reference
				b_{abs_365} (Mm^{-1})	MAE_{365} ($m^2\ g^{-1}$)	AAE	b_{abs_365} (Mm^{-1})	MAE_{365} ($m^2\ g^{-1}$)	AAE	
Qinghai lake	3200 m	Himalayas and Tibetan Plateau (HTP), China	Monsoon	1.9 ± 0.5	1.6 ± 0.7	5.7	2.2 ± 1.0	0.7 ± 0.3	6	Zhu et al., 2024
			Post-monsoon	2.8 ± 1.2	1.0 ± 0.2	5.7	4.1 ± 2.3	0.6 ± 0.1	6.6	
			Winter	3.3 ± 1.0	1.5 ± 0.3	5.5	4.7 ± 1.7	0.7 ± 0.2	6.7	
			Pre-monsoon	3.4 ± 1.0	1.4 ± 0.6	5.4	3.8 ± 2.3	0.7 ± 0.2	6	
Ngari	4360 m		Monsoon	2.5 ± 1.9	2.3 ± 1.1	5.7	3.7 ± 4.7	0.7 ± 0.4	6	
			Post-monsoon	4.6 ± 2.5	4.2 ± 1.7	6.3	12.0 ± 16.4	1.2 ± 0.9	8.1	
			Winter	5.4 ± 1.7	3.7 ± 0.6	6.5	9.2 ± 8.7	1.3 ± 0.2	7.9	
			Pre-monsoon	2.7 ± 1.0	2.6 ± 0.7	6.2	3.4 ± 1.5	0.7 ± 0.1	6.1	
Purang	3952 m		Monsoon	1.2 ± 0.4	4.1 ± 1.4	6.5	2.7 ± 2.0	0.8 ± 0.3	6.6	
			Post-monsoon	2.0 ± 0.5	3.5 ± 0.7	5.6	2.9 ± 0.6	0.6 ± 0.1	4.9	
			Winter	3.3 ± 1.1	4.6 ± 0.9	6.7	6.4 ± 2.9	1.0 ± 0.1	6.6	
			Pre-monsoon	7.7 ± 7.5	4.1 ± 1.0	6.7	8.6 ± 6.0	0.8 ± 0.1	6.7	
Beiluhe	4659 m		Monsoon	0.6 ± 0.0	2.4	4.6	0.3 ± 0.2	0.3	4.4	
			Post-monsoon	0.6 ± 0.4	2.8 ± 0.0	5.9	0.7 ± 0.7	0.3 ± 0.1	5.4	
			Winter	0.7 ± 0.3	2.6 ± 0.3	5.5	0.4 ± 0.4	0.2 ± 0.2	3.2	
			Pre-monsoon	0.6 ± 0.1	2.5 ± 0.9	5.4	0.3 ± 0.1	0.2 ± 0.0	4.1	
Lachung, Sikkim	2700 m	Eastern Himalayan region, India	Spring	5.9 ± 4.2	1.5 ± 0.6	4.1 ± 0.7	9 ± 4.6	2.1 ± 0.8	5.2 ± 1.8	Arun et al., 2024
			Summer	1.7 ± 0.5	1.0 ± 0.3	4.1 ± 1.8	3.4 ± 1.4	1.4 ± 0.5	4.6 ± 1.0	
			Autumn	2.4 ± 1.1	0.79 ± 0.2	4.8 ± 1.5	4.6 ± 2.3	1.0 ± 0.4	5.1 ± 0.6	
			Winter	4.4 ± 1.7	0.75 ± 0.2	5.5 ± 0.9	7.4 ± 1.8	0.9 ± 0.2	6.3 ± 1.5	
Lulang	3326 m	Tibetal Plateau, China	Winter	1.04 ± 0.25	0.75±0.13	6.7±0.8	1.47 ± 0.51	0.71±0.16	8.2±1.4	Zhu et al., 2018
			Pre-monsoon	0.85 ± 0.25	0.62±0.09	6.6±0.6	0.97 ± 0.24	0.51±0.12	8.4±0.9	
			Monsoon	0.38 ± 0.09	0.32±0.07	7.2±0.9	0.67 ± 0.17	0.27±0.06	8.1±0.9	

			Post-monsoon	0.55 ± 0.23	0.44±0.14	7.7±1.3	1.09 ± 0.15	0.58±0.05	8.0±1.0	
Bode (Kathmandu)	1300 m	Central Himalayan region, Nepal	Pre-monsoon	23.2 ± 11.3	1.4 ± 0.2	4.8 ± 0.4	-	-	-	Chen et al., 2020
			Monsoon	11.5 ± 7.79	1.0 ± 0.3	4.2 ± 0.6	-	-	-	
			Post-monsoon	17.0 ± 10.1	1.2 ± 0.2	4.9 ± 0.3	-	-	-	
			Winter	20.4 ± 14.0	1.5 ± 0.2	5.1 ± 0.3	-	-	-	
			Annual	17.5 ± 12.2	1.4 ± 0.3	4.6 ± 0.8	-	-	-	
ICIMOD site, Godavari	1600 m	Central Himalayan region, Nepal	Winter	-	1.05 ± 0.21	5.18 ± 0.33	-	-	-	Wu et al., 2019
			Pre-monsoon	-	0.59 ± 0.16	5.16 ± 0.68	-	-	-	
			Monsoon	-	0.83 ± 0.10	5.31 ± 0.18	-	-	-	
			Post-monsoon	-	0.83 ± 0.09	5.35 ± 0.40	-	-	-	
			Annual	-	0.77 ± 0.23	5.23 ± 0.52	-	-	-	
SETS (SE Tibet)	3326 m	Tibetan Plateau, China	Summer	-	0.27 ± 0.10	7.22 ± 1.45	-	0.34 ± 0.12	5.53 ± 1.04	Wu et al., 2020
			Winter	-	0.86 ± 0.17	5.92 ± 0.43	-	0.59 ± 0.44	6.24 ± 1.24	
Nam Co Lake	4730 m	Tibetan Plateau, China	Pre-monsoon	0.22 ± 0.05	0.46 ± 0.08	6.57 ± 0.56	-	-	-	Zhang et al., 2017
			Monsoon	0.09 ± 0.05	0.32 ± 0.18	5.91 ± 2.14	-	-	-	
			Average	0.15 ± 0.08	0.38 ± 0.16	6.19 ± 1.70	-	-	-	
Nainital	1950 m	Central Himalay region, India	Winter	17.7±13.3	-	-	-	-	-	Ram et al., 2010
			Pre-monsoon	11.3±5.8	-	-	-	-	-	
			Post-monsoon	17.6±13.3	-	-	-	-	-	
NCO-P, Khumbu valley	5079 m	Central Himalay region, Nepal	Pre-monsoon	1.83 ± 1.46	0.72 ± 0.15	5.1 ± 0.3	2.86 ± 2.49	0.77 ± 0.18	3.9 ± 0.5	Kirillova et al., 2016
			Monsoon	0.21 ± 0.22	0.45 ± 0.18	4.2 ± 0.6	0.32 ± 0.29	0.51 ± 0.15	4.4 ± 1.4	
			Post-monsoon	0.3	0.36	5.6	0.72	0.65	3.3	
			Winter	0.31 ± 0.08	0.61 ± 0.08	5.4 ± 0.6	0.61 ± 0.20	0.71 ± 0.13	3.8 ± 0.8	
Lumbini	100 m	Central Himalay region, Nepal	Pre-monsoon	-	1.81±0.34	3.98±0.39	-	-	-	Chen et al., 2020
			Monsoon	-	1.31±0.33	4.75±0.60	-	-	-	
			Post-monsoon	-	1.28±0.21	4.37±0.88	-	-	-	
			Winter	-	1.41±0.46	5.50±0.38	-	-	-	
			Annual	-	1.52±0.41	4.47±0.74	-	-	-	
		Western	Summer	-	0.05 ± 0.03	0.59 ± 0.36	-	-	-	

		Himalayan region, India	Winter	-	0.07 ± 0.04	0.36 ± 0.47	-	-	-
			Average	-	0.06 ± 0.02	0.47 ± 0.16	-	-	-
Gangotri Gomukh glacier	3415 m	Central Himalayan region, India	Summer	-	0.16 ± 0.05	1.61 ± 0.66	-	-	-
			Winter	-	0.17 ± 0.04	1.44 ± 0.35	-	-	-
			Average	-	0.16 ± 0.01	1.53 ± 0.12	-	-	-
Zemu glacier	2700 m	Eastern Himalayan region, India	Summer	-	0.12 ± 0.03	1.39 ± 0.35	-	-	-
			Winter	-	0.11 ± 0.01	1.38 ± 0.59	-	-	-
			Average	-	0.12 ± 0.01	1.38 ± 0.01	-	-	-

Table S7. Cluster contribution to $b_{abs\_aq\_365}$, MAE_{365}, and AE across seasons at 1000 m above ground level (AGL).

1000 m AGL	**(Local+ Regional)**			**(Long range)**		
Parameters	**b_{abs} (Mm^{-1})**	**MAE ($m^2\ g^{-1}$)**	**AAE**	**b_{abs} (Mm^{-1})**	**MAE ($m^2\ g^{-1}$)**	**AAE**
Summer	2.8 ± 1.1	0.7±0.3	6.6±0.5	2.5±0.8	1.1±0.5	6.2±0.7
Post-monsoon	3.4 ± 2.0	1.0±0.5	6.6±0.3	4.7±2.5	0.9±0.2	6.4±0.3
Winter	17.2±8.3	1.8±0.4	6.0±0.1	14.4±6.4	1.9±0.5	5.9±0.2

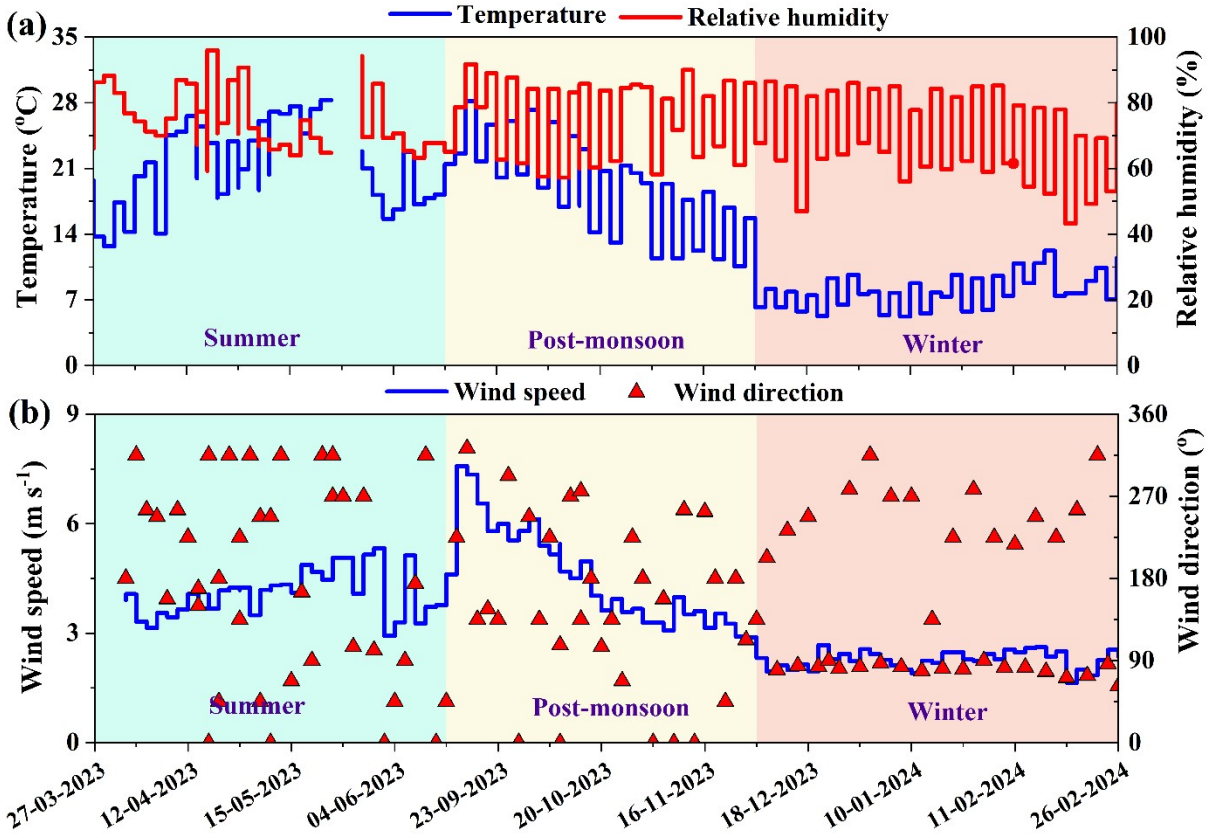

Figure S1. Time series of (a) temperature and relative humidity, and (b) wind speed and wind direction during the sampling period.

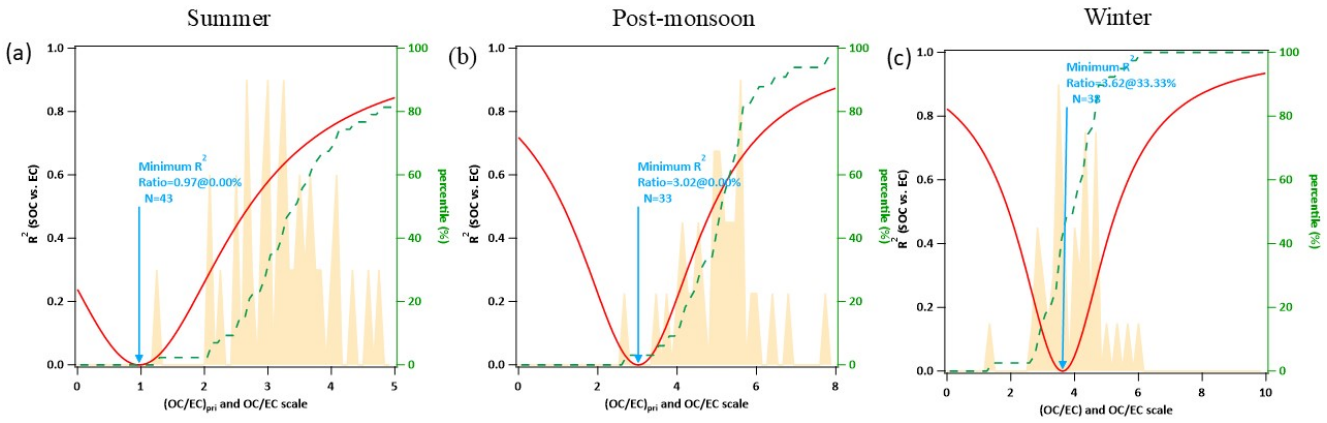

Figure S2. Determination of $(OC/EC)_{pri}$ using the minimum R^2 method (MRS) for (a) summer, (b) post-monsoon, and (c) winter. The red curve shows the coefficient of determination (R^2) between SOC and EC as a function of assumed $(OC/EC)_{pri}$. The shaded area represents the frequency distribution of the OC/EC ratio for each season, and the green dashed curve is the cumulative frequency curve of the OC/EC ratio.

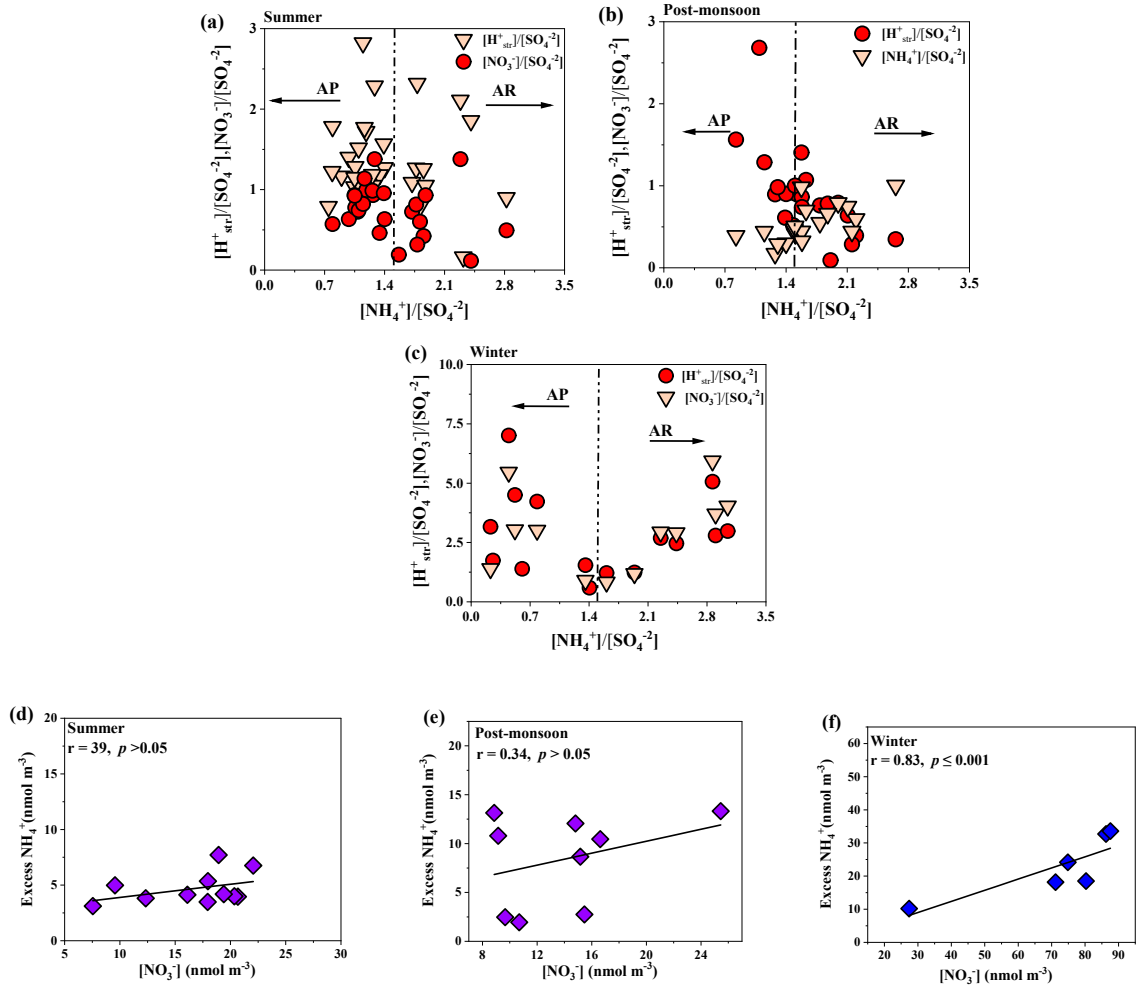

Figure S3. Scatter plots of $[H^+_{str}]/[SO_4^{-2}]$ and $[NO_3^-]/[SO_4^{-2}]$ vs $[NH_4^+]/[SO_4^{-2}]$ for (a) summer, (b) post-monsoon season and (c) winter seasons. Associations between NO_3^- and excess ammonium for (d) summer, (e) post-monsoon season and (f) winter are also shown. Here, H^+_{str} refers to strong acidity, and is calculated as $(2 \times SO_4^{2-} + NO_3^-) - NH_4^+$.

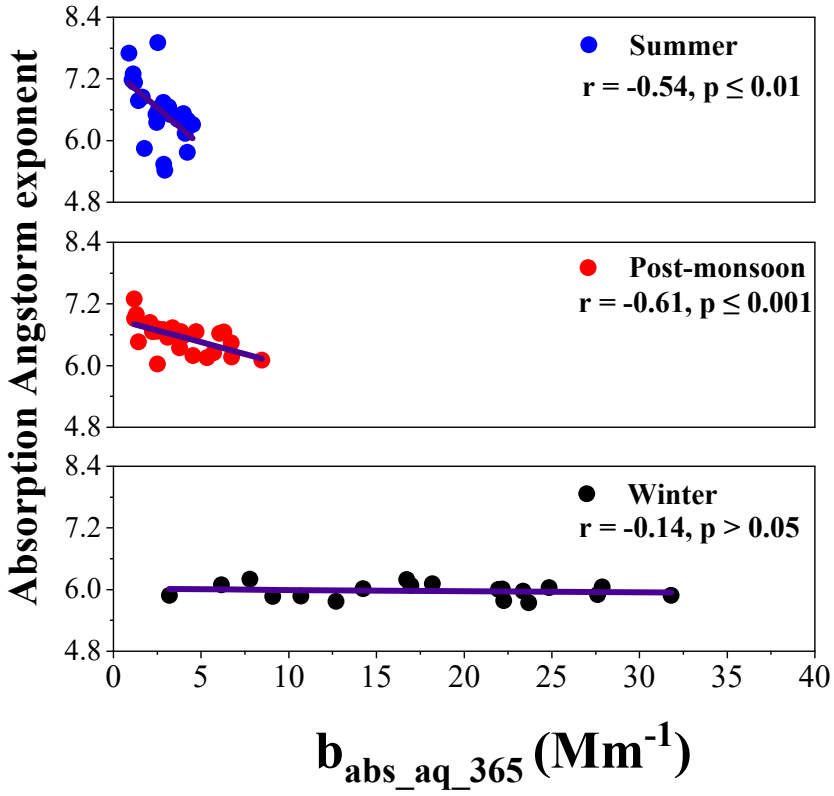

Figure S4. Correlation between $b_{abs\_aq\_365}$ and Angstrom exponent.

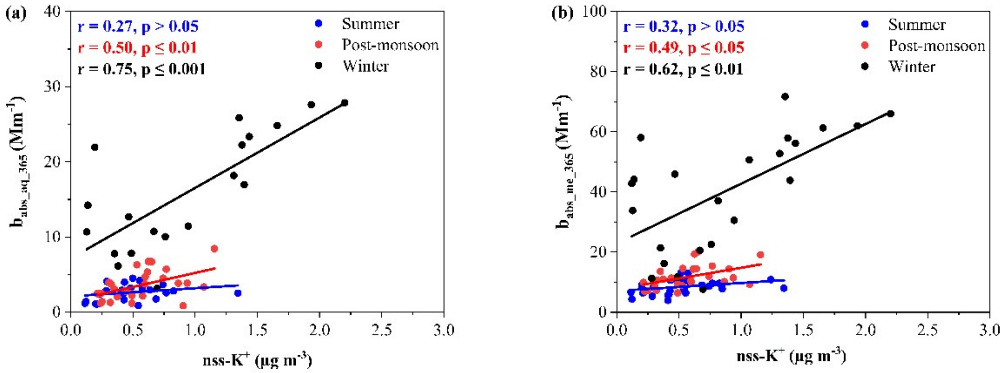

Figure S5. Correlation between nss-K^+ and b_{abs_365} of BrC_{aq} (a) and BrC_{me} (b) for the three seasons.

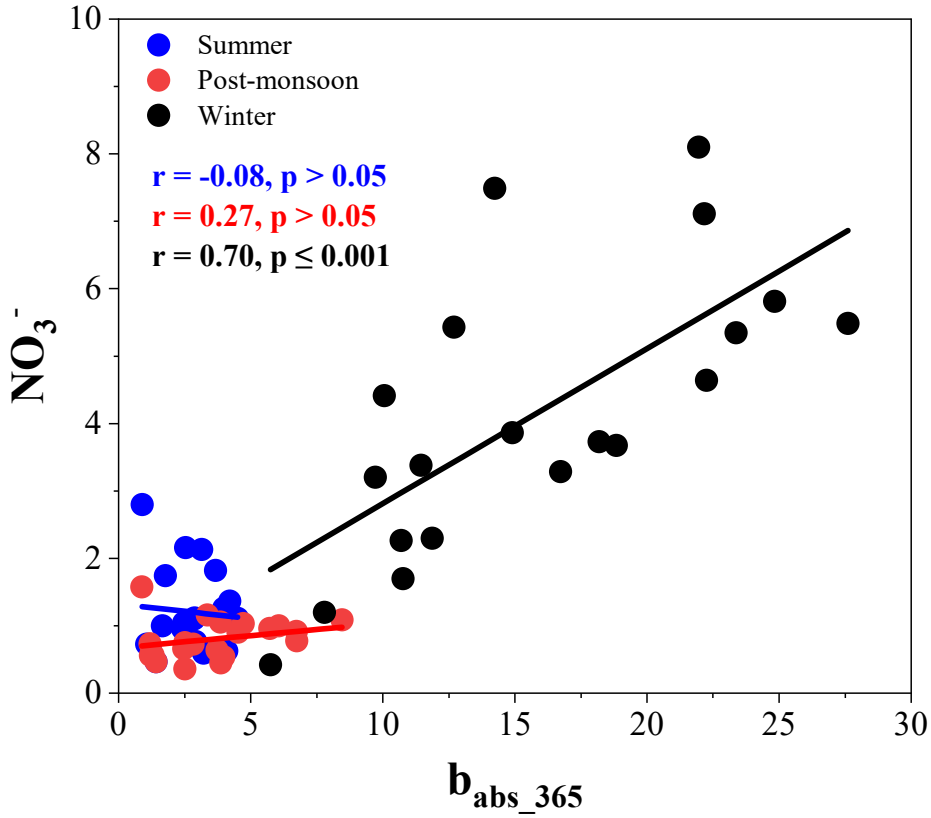

Figure S6. Correlation between $b_{abs\_aq\_365}$ and NO_3^- for the three seasons.

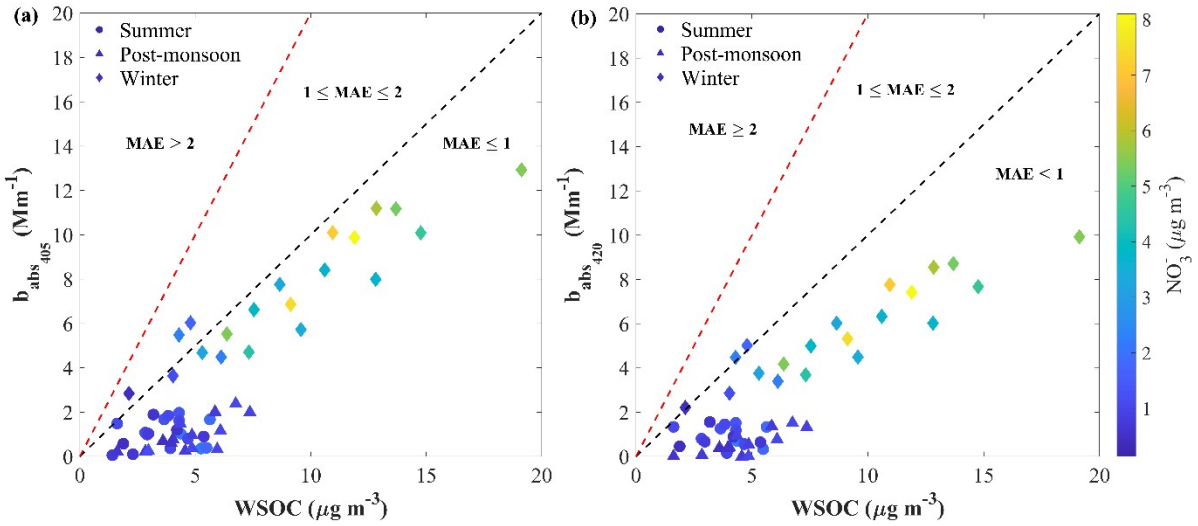

Figure S7. Scatter plot between WSOC and $b_{abs\_aq\_405}$ (a) and WSOC vs $b_{abs\_aq\_420}$ (b) across the seasons. The dashed black and red lines represent MAE = 1 and MAE = 2, respectively.

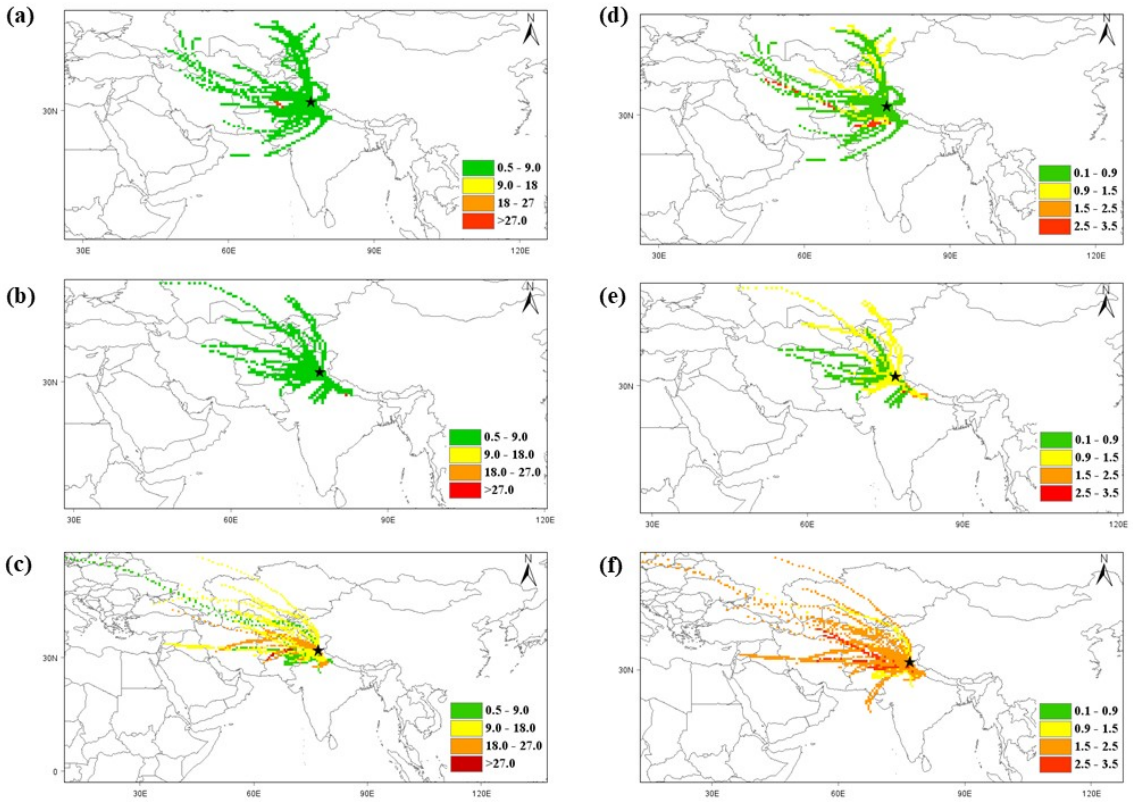

Figure S8. Concentration weighted trajectories (CWTs) of $b_{abs\_aq\_365}$ at 1000 m AGL for the summer (a), post-monsoon (b), and winter (c) seasons and MAE_{365} at 1000 m AGL for the summer (d), post-monsoon (e), and winter (f) seasons.

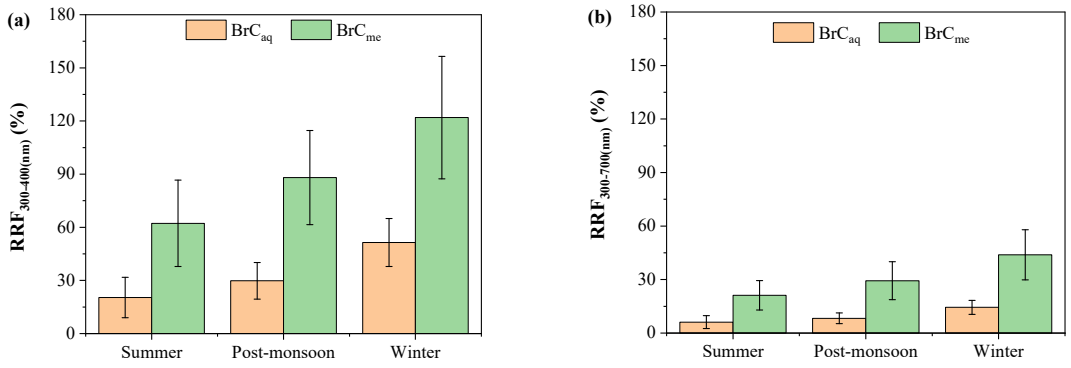

Figure S9. Relative radiative forcing for 300-400 nm wavelength range (a) and 300-700 nm wavelength range for BrC_{aq} and BrC_{me} across seasons.

References

Arun, B. S., Gogoi, M. M., Deshmukh, D. K., Hegde, P., Boreddy, S. K. R., Borgohain, A., & Babu, S. S. (2024). Enhanced light absorption by ambient brown carbon aerosols in the eastern Himalayas. *Environmental Science: Atmospheres*, *4*(7), 782–801. https://doi.org/10.1039/d4ea00021h

Chen, P., Kang, S., Tripathee, L., Ram, K., Rupakheti, M., Panday, A. K., Zhang, Q., Guo, J., Wang, X., Pu, T., & Li, C. (2020). Light absorption properties of elemental carbon (EC) and water-soluble brown carbon (WS–BrC) in the Kathmandu Valley, Nepal: A 5-year study. *Environmental Pollution*, *261*. https://doi.org/10.1016/j.envpol.2020.114239

Kirillova, E. N., Marinoni, A., Bonasoni, P., Vuillermoz, E., Facchini, M. C., Fuzzi, S., & Decesari, S. (2016). Light absorption properties of brown carbon in the high Himalayas. *Journal of Geophysical Research: Atmospheres*, *121*(16), 9621–9639. https://doi.org/https://doi.org/10.1002/2016JD025030

Ram, K., Sarin, M. M., & Hegde, P. (2010). Long-term record of aerosol optical properties and chemical composition from a high-altitude site (Manora Peak) in Central Himalaya. *Atmospheric Chemistry and Physics*, *10*(23), 11791–11803. https://doi.org/10.5194/acp-10-11791-2010

Verma, S. R., Pervez, S., Chow, J. C., Watson, J. G., Andrabi, S. M., Mandal, P., Khan, N. A., Tiwari, S., Chandra Dumka, U., Chakrabarty, R. K., Verma, M., Pervez, Y. F., Mishra, A., Tamrakar, A., Sowmya, H. N., Deb, M. K., Ghosh, K. K., Jain, V. K., Karbhal, I., … Satnami, M. L. (2023). Optical Properties of Fine Mode Aerosols over High-Altitude Himalayan Glacier Regions. *ACS Earth and Space Chemistry*, *7*(8), 1536–1544. https://doi.org/10.1021/acsearthspacechem.3c00088

Wu, G., Ram, K., Fu, P., Wang, W., Zhang, Y., Liu, X., Stone, E. A., Pradhan, B. B., Dangol, P. M., Panday, A. K., Wan, X., Bai, Z., Kang, S., Zhang, Q., & Cong, Z. (2019). Water-

Soluble Brown Carbon in Atmospheric Aerosols from Godavari (Nepal), a Regional Representative of South Asia. *Environmental Science and Technology*, *53*(7), 3471–3479. https://doi.org/10.1021/acs.est.9b00596

Wu, G., Wan, X., Ram, K., Li, P., Liu, B., Yin, Y., Fu, P., Loewen, M., Gao, S., Kang, S., Kawamura, K., Wang, Y., & Cong, Z. (2020). Light absorption, fluorescence properties and sources of brown carbon aerosols in the Southeast Tibetan Plateau. *Environmental Pollution*, *257*, 113616. https://doi.org/https://doi.org/10.1016/j.envpol.2019.113616

Zhang, Y. G., Xu, J. Z., Shi, J. Sen, Xie, C. H., Ge, X. L., Wang, J. F., Kang, S. C., & Zhang, Q. (2017). Light absorption by water-soluble organic carbon in atmospheric fine particles in the central Tibetan Plateau. *Environmental Science and Pollution Research*, *24*(26), 21386–21397. https://doi.org/10.1007/s11356-017-9688-8

Zhu, C. S., Cao, J. J., Huang, R. J., Shen, Z. X., Wang, Q. Y., & Zhang, N. N. (2018). Light absorption properties of brown carbon over the southeastern Tibetan Plateau. *Science of the Total Environment*, *625*, 246–251. https://doi.org/10.1016/j.scitotenv.2017.12.183

Zhu, C. S., Qu, Y., Huang, H., Shi, J. L., Dai, W. T., Zhang, N. N., Wang, N., Wang, L. Y., Ji, S. S., & Cao, J. J. (2024). Brown Carbon From Biomass Burning Reinforces the Himalayas and Tibetan Plateau Warming. *Geophysical Research Letters*, *51*(9). https://doi.org/10.1029/2023GL107269